1003-7713/2004/03-346-11

以交叉分子束及时间切片离子速度成像法研究产物成对相关讯息*

林志民， 周金刚， 徐维成， 刘国平**
（中央研究院原子与分子科学研究所，台北市 106）

摘 要： 研发了一种新颖的实验方法，用以在交叉分子束条件下测量双分子反应产物的成对相关（pair correlation）讯息. 作为尝试，首先选取了 $F + CD_4/CHD_3/CH_4$ 反应体系. 结合时间切片离子速度成像与交叉分子束技术，可直接测得产物态分辨且成对相关的角分布. 已研究了产物成对相关的几个方面，阐释了碰撞能效应. 测量表明，产物角分布对 HF/DF 产物振动态有极强的相关性，同时对甲基产物的振动态也有不可忽视的相关性. 在低碰撞能时，在 $F + CH_4$ 多原子反应中，首度发现了反应动态共振的证据.

关键词： 产物成对相关性；离子速度成像；密度-通量转换；反应共振
中图分类号： O64 **文献标识码：** A

Product Pair-correlation by Crossed Molecular Beam and Time-sliced Ion Velocity Imaging Methods*

Lin Jim Jr-Min, Zhou Jingang, Shiu Wei-Chen, Liu Kopin**
(*Institute of Atomic and Molecular Sciences* (*IAMS*), *Academia Sinica*, *Taipei*, 106)

Abstract A novel experimental technique has been developed to measure the attributes of product pair correlation of bimolecular reactions under the crossed molecular beam condition. The first system that we picked is $F + CD_4/CHD_3/CH_4$ reactions. By combining a crossed molecular beam method with a time-sliced ion velocity imaging technique, the product state-resolved pair-correlated differential cross sections were revealed directly from the measurements. Several facets of the product pair correlation have been explored. The dependence on the collisional energy has been elucidated. The pair-correlated angular distributions show strong dependences on the HF/DF vibrational quantum numbers, and weaker yet not negligible dependences on the methyl radical vibrational quantum numbers. For the $F + CH_4$ reaction at collisional energies close to the reaction threshold, the first experimental evidences of a reactive resonance in a polyatomic reaction were discovered. The product pair-correlated information helps us to unravel the complexity of polyatomic reactions and offers the important link between A + BC type of reactions and more general polyatomic reactions.

Keywords Product pair correlation, Ion velocity imaging, Density-to-flux transformation, Reactive resonance

---

* Dedicated to the 80th birthday of Professor Qihe Zhu.

** Corresponding author, E-mail：kpliu@gate.sinica.edu.tw Received 15 March 2004.

1 Introduction

Reaction dynamics is essentially the modern-day approach to the study of reaction kinetics[1,2]. The fundamental aim is to understand the intimate mechanisms of chemical reactivity at a microscopic level of detail. To understand the detailed mechanism of an elementary reaction, we rely on both experimental observations and theoretical calculations. For example, the state distributions of the products, the collisional energy dependence, the product angular distributions, etc. could be measured experimentally. Combined with theoretical investigations, *ab initio* calculations and models, the mechanism of the reaction can hopefully be understood. For a chemical reaction, the critical region is the transition state that separates the products from the reactants. This critical region is believed to be the most important, yet least understood aspect. The goal of chemical dynamics studies is to comprehend the behavior of the reacting system in this elusive critical region microscopically, such as the interaction between atoms, the energy flow and redistribution, the steric effects, etc.

Crossed molecular beam experiments that measure the state-resolved product angular distributions at a well-controlled collisional energy can provide important data for dynamics studies. Recently, thanks to the significant progresses of both theoretical calculations and experimental techniques, quantitative understanding of a few simple systems has been achieved. These benchmark systems are H + H_2 (or HD, D_2)[3-6], F + H_2[7-9], O(^{1}D) + H_2[10], and OH + H_2[11]. Precise measurements and high level quantum calculations can be compared with each other. Proper interpretations can then be put forward. For reactions of similar sizes (number of atoms and electrons involved), the results can be largely predicted, provided that the interaction potential is sufficiently accurate.

Of course, we should not limit the studies of reaction dynamics to just three- or four-atom systems. The three-atom and four-atom systems have too few degrees of freedom (DOF) to be extrapolated to a more general polyatomic system. As the number of atoms increases, the number of the DOF increases dramatically. For example, for a system of n atoms, there are N degrees of vibrational freedom and $N = 3n - 6$ if the structure is nonlinear. Thus, there are 3 DOF for a three-atom system, 6 DOF for a four-atom system, 9 DOF for a five-atom system, and so on. If we wish to calculate a potential energy surface that samples 10 points in every DOF, we need 10^N points for a system of N-DOF, which can become prohibitively large even using the best computer resources. Fortunately, a polyatomic system ($n > 4$) often involves a very high density of states, —too dense to be resolved experimentally. To understand the dynamical behavior of a reaction, what is more important is to have a resolution that is high enough to resolve the relevant dynamical attributes. A full resolution experiment may not necessarily be essential. For example, it is often not necessary to resolve all the individual rovibrational state, while it is important to know the averaged vibrational and rotational energy releases. If we merely measure the total internal energy with a too low resolution that the vibrational states can not be separated from the overlaps of their rotational envelopes, it will be hard to retrieve the correct vibrational distribution, even for the averaged vibrational energy. More importantly, not all DOF affect the reaction in the same manner. For example, the concept of functional groups is to limit the reactive part of a molecule to a small group of atoms. Also, only certain vibrational mode excitations help to carry the reaction system across the barrier. Concepts like functional groups and reaction centers are quite common in synthetic chemistry (organic and inorganic chemistry). For a more precise field of physical chemistry[12], what we need is to build up the similar backbone knowledge to better interpret polyatomic reactions, and eventually to predict the outcomes reliably.

The reaction of fluorine atom with methane, F + $CH_4 \rightarrow HF + CH_3$, is an attractive prototype for this endeavor. First, it is a direct reaction in which the product state distributions can sensitively reveal the key features of the potential energy surface. In contrast, if a reaction goes through a long-lived intermediate, its product distribution is often statistical-like. Secondly,

there are vibrational and rotational states of the two molecular products. Besides rotational motions, HF has only one vibrational DOF while CH_3 has 6 vibrational DOF that belong to 4 vibrational normal modes. Which vibrational modes will be excited during this reaction? What is the mode/state correlation of the coincidently formed HF + CH_3 product pairs? Such questions are beyond the three-atom reaction. Furthermore, there exists a dynamical resonance in the F + HD → HF + D reaction[7-9,13]. In view of the fast time scale of the intramolecular vibrational dynamics, can this facinating quantum phenomenon exist at all in a polyatomic reaction? This question is very intriguing, yet hitherto unaddressed.

In this contribution, a pedagogic account of our approach toward understanding polyatomic reaction dynamics will be presented, emphasizing the basic ideas and fundamental elements. The remaining part of this paper is organized as following. First, we explain the experimental observables of a crossed molecular beam reaction, using F + CH_4 reaction as an example. Secondly, we describe the experimental setup. A novel three-dimensional ion velocity imaging technique has been developed for this study. Finally, the product mode correlation is discussed and a few results are reviewed.

2 A few experimental observables

The reaction cross section (σ) is the microscopic reaction probability (summed over all impact parameters or partial waves), which can be linked to the macroscopic rate constant as $k = v_r\sigma$ in a bimolecular reaction, where v_r is the relative velocity of the two reactant molecules. The collisional energy dependence of the reaction cross section is called the excitation function, $\sigma(E_c)$. A molecular beam has narrow speed and angular distributions. A crossed molecular beam reaction has a well-defined collisional energy, hence, is ideal for studying the excitation function. Since the reaction cross section becomes zero or very small when the collisional energy is less than the reaction barrier, the excitation function can reveal the magnitude of the reaction barrier. The shape of the excitation function, on the other hand, depends on the reaction mechanism and is sensitive to the entrance region of the reaction[14].

If the product velocity distribution is measured, the translational energy distribution can be derived. By conservation of energy and linear momentum, the total internal energy distribution of the products can be deduced. Using F + CH_4 → HF + CH_3 as an example,

$$E_{\text{trans}} = \frac{1}{2} m_{\text{HF}} u_{\text{HF}}^2 + \frac{1}{2} m_{\text{CH}_3} u_{\text{CH}_3}^2 \quad (1)$$

$$m_{\text{HF}}\mathbf{u}_{\text{HF}} + m_{\text{CH}_3}\mathbf{u}_{\text{CH}_3} = 0 \quad (2)$$

$$E_{\text{total}} = E_c - \triangle H_0^0 = E_{\text{trans}} + E_{\text{int}} \quad (3)$$

where E_{trans} is the total product translational energy, $\mathbf{u}$ is the product recoil velocity vector in the center-of-mass frame, and $-\triangle H_0^0$ is the reaction exothermicity. By momentum conservation, only the velocity vector of one product needs to be measured and that of the other concomitant product can be calculated from equation (2). The internal energy has two parts, $E_{\text{int}} = E_{\text{int}}(\text{HF}) + E_{\text{int}}(\text{CH}_3)$. The combinations of the internal energy levels of the two product molecules are enormous and too dense to be resolved by merely measuring of the total translational energy distribution. A state-selective probe of the CH_3 products is then desired. A resonance-enhanced multiphoton ionization (REMPI) probe can select the internal state(s) of the CH_3 products[15], thus fix $E_{\text{int}}(\text{CH}_3)$. From

$$E_{\text{int}}(\text{HF}) = E_{\text{total}} - E_{\text{trans}} - E_{\text{int}}(\text{CH}_3) \quad (4)$$

the relatively sparse rovibrational levels of HF can hopefully be resolved in the CH_3 state-selective product translation energy distributions, provided that E_{trans} is measured with sufficient resolution.

The partition of the product energy offers the information of the energy flow while the reaction is taking place. It is obvious that translational, rotational, or vibrational energy excitation of the products should come from different microscopic mechanisms. It has been known that the energy disposal depends sensitively on the geometry of the transition state and the kinematics (the mass factor and conservation laws of energy, parity, and angular momentum). The energy partition between the vibrational modes reveals important dynamics of the reaction, especially in the case of a polyatomic system of multiple vibrational modes. One limiting case

is that all energy is distributed randomly among all modes, the statistical case. Another common case is that the energy is constrained within certain motion of atoms, which leads to only a few modes being active during the reaction.

The product angular distributions also provide important information. The angular distribution refers to the product formation probability per unit solid angle. As above, we use the symbol of the reaction cross section, σ, for the probability of product formation. The angular distribution can be expressed as $d\sigma(\theta,\phi)/d\Omega$ in a polar coordinate and $d\Omega = \sin\theta d\theta d\phi$. Owing to the randomness of the impact parameters, the reaction system (for unpolarized reactants) should exhibit a cylindrical symmetry around the relative velocity vector, i. e. , $d\sigma/d\phi$ = constant when we choose the relative velocity direction as the symmetry axis. Thus, the angular distribution can be expressed as $d\sigma/\sin\theta d\theta$ or $d\sigma/d\cos\theta$, which is usually called differential cross section from this differential form of expression.

In a scattering event, the impact parameter is the shortest distance of the colliding pair in the absence of intermolecular interactions. In analogy to a baseball game, the impact parameter gauges how accurately the bat hits the ball. Similarly, the angular distribution of the scattered products depends on the value of the impact parameters. For a direct, hard-sphere like reaction, small impact parameters lead to backward scattering, while large impact parameters yield forward scattering[2,16]. Usually not every collisional event can react. The product angular distribution indicates the success rate of various impact parameters. If only backward products are observed, the collisions with larger impact parameters just fail to react.

3　Experimental setup

3.1　Crossed molecular beam setup

The CH_4 supersonic jet was generated by expanding 70 psig neat CH_4 gas though a pulsed valve of 0.5 mm orifice into a vacuum chamber. The supersonic expansion[17] cools the translational and rotational motions of CH_4 quite effectively. Usually, the translational and rotational temperatures can be in the order of 10 K and it is not difficult to achieve 2 ~ 3 K, while the vibrational degrees of freedom are more difficult to relax due to the smaller V-T and V-R relaxation cross sections. A skimmer of 3 mm diameter is used to skim the center cone of the jet to form a molecular beam. The speed of methane beam is about 1 ~ 1.2 km/s depending on the isotopic variants (CH_4, CHD_3, CD_4) used.

The F-atom beam was generated by introducing a glow discharge through a F_2/He mixture in the expansion region of a piezoelectric pulsed valve[18]. The glow discharge takes place between two stainless steel plates with a ceramic spacer in between. These three plates have holes of 1.5 mm diameter in the center. The plate thickness is about 2 mm. A 1.5 mm diameter channel is formed by stacking these three plates together. When the pulsed gas mixture passes through the discharge channel, a high voltage pulse (~1 kV) is applied to one of the electrodes to induce the glow discharge. Metastable He^* is formed in the plasma, in which complicated chemistry is involved. The following reactions are just few examples:

$$He + e^- \rightarrow He^* + e^- \quad (5)$$

$$He^* + F_2 \rightarrow 2F + He \quad (6)$$

$$He^* + M \rightarrow He + M \quad (7)$$

The residual He^* may interfere the crossed beam reaction of interest. For instance,

$$He^* + CH_4 \rightarrow CH_4^* + He \quad (8)$$

and CH_4^* can be field ionized by the electric field of the ion optics, or photoionized by the laser beam. Most of the ion background is CH_4^+, but still some CH_3^+ are present when He^* concentration is high. The amount of He^* depends on the F_2 concentration, gas pressure, discharge current, electrode surface conditions, etc. Acidic treatment (e.g. using 20% $HNO_{3(aq)}$) of the stainless steel electrodes is necessary to keep a stable discharge. For generating a short but concentrated F atom pulsed beam, a high voltage transistor switch is used to control the discharge pulse of 60 mA and 15 μs width at the optimized timing in the gas pulse. By carefully adjusting the delay time, discharge current, gas pressure, etc, the optimized condition can be achieved, i. e. maximum F atom concen-

tration and minimum metastable rare gas concentration[19]. A 5% F_2/He or F_2/Ne gas mixture is used. A too diluted mixture results in too many metastable rare gas atoms. A too concentrated mixture will give a broad speed distribution of the molecular beam and will not yield higher F atom concertration. In the present study, the F atom speed is about 1.7 km/s for 5% F_2/He mixture, and about 1 km/s for 5% F_2/Ne mixture.

Fig. 1 shows the experimental configuration. The two molecular beams and the laser beam are all in the same plane. Two molecular beam source chambers can be rotated independently. By varying the intersection angle between the two molecular beams, the relative velocity of the reactants can be changed to give different collisional energies.

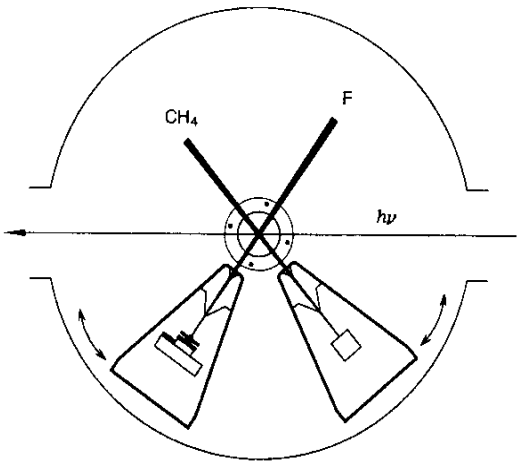

Fig. 1 The schematic experimental setup

The two molecular beams and the laser beam are in the same plane. Two molecular beam source chambers can be rotated independently to change the intersection angle between the two beams. The ion flight axis is perpendicular to the molecular beam plane.

Two reactant beams cross each other at the center. For a molecular beam of a typical density, the probability of secondary collisions is much smaller than the probability of reactive scattering. In other words, almost all products observed are nascent. Here the CH_3 products are probed by a 2 + 1 REMPI scheme via the $3p_z$ intermediate state. In a photoionization process, most of the excess energy is carried away by the photoelectron and the speed of the cation is almost the same as the neutral molecules because of the large mass disparity between the electron and the cation. The velocity distributions of the nascent CH_3 products are measured by recording the CH_3^+ ion velocity imaging.

3.2 Concept of ion velocity imaging

The early approach of ion imaging[20,21] may be simply described as follows: a homogeneous electric field (the field vector is set to the z direction, thus $E_x = E_y = 0$) is used to extract the ions. The x and y components of the ion velocity vector (v_x, v_y) are not affected by this extraction field. So

$$x_d = x_0 + v_x t \tag{9}$$

where x_d is the position x component on the detection plane, x_0 is the ion initial position, and t is the ion time of flight (TOF). When the spread of x_0 is very small (point ion source), the distribution of (x_d, y_d) shows the distribution of (v_x, v_y), since t is almost a constant for a given mass. Practically, the size of ion source is usually limited by the signal strength and the laser beam size, $x_d > \sim 1$ mm. The size of the ion detector limits the maximum value of x_d to be within 20 mm for a commercially available image detector. The combination of both makes the velocity resolution worse than 5%. The image measured by this method is a compressed image containing two-dimensional velocity information, since there is no distinction for the v_z component.

In 1997, Eppink and Parker reported an innovative velocity mapping method[22]. This method utilizes the focusing power of ion optics to reduce the effect of the spread of x_0 such that

$$x_d = Fx_0 + Mv_x t \tag{10}$$

where F is the spatial focus ratio and M is the velocity magnifying factor. Practically, F can be as small as 0.05 and M is close to 1. Thus, the velocity resolution can be improved significantly. Nowadays, about 1% velocity resolution can be achieved routinely in many laboratories. The effect of the velocity mapping is exemplified here. Under the mapping condition, F is much less than 1 and the ion velocity distribution can be imaged with high resolutions as illustrated in Fig. 2a and Fig. 2b. On the other hand, when the ion optics voltages are set to give a homogeneous electric field such that F is about 1 —the spatial-mode operation,

and the resultant ion images are shown at Fig. 2 c and d. As can be seen, a significant contribution from the spatial distribution of the probe laser is apparent, which distorts the images and worsens the velocity distribution.

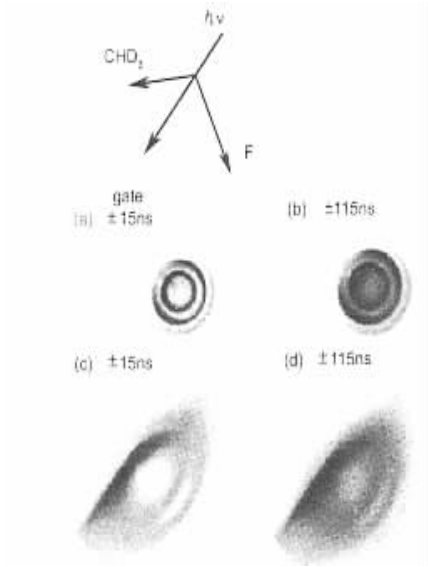

Fig. 2　Raw CHD_2 ($v=0$) product ion images showing the effects of ion velocity mapping and time slicing (a) with both velocity mapping and time slicing, (b) with velocity mapping but without time slicing (conventional velocity mapping), (c) without velocity mapping but with time slicing, and (d) without velocity mapping and without time slicing. In (c) and (d), the spatial distribution of the ion cloud can be seen (thus, named "spatial-mode" operation.

For more precise and direct measurement of ion velocities, we develop a novel three-dimensional velocity imaging technique[19]. Our approach is to utilize the ion TOF to map out the v_z component[23] while keeping the velocity mapping condition for v_x and v_y. This v_z-to-t mapping is by taking advantage of the ion turn-around-time (t_r) under a homogeneous electric field, which can be expressed as

$$t_r = -\frac{v_z}{a_z} = -\frac{mv_z}{qE_z} \qquad (11)$$

$$t = t_0 + t_r \qquad (12)$$

where m/q is the mass-to-charge ratio of the ion, a_z is the external acceleration, E_z is the z component of the extraction electric field strength, and t_0 is the ion TOF for $v_z=0$. It is clear that for a given v_z, the smaller E_z the larger t_r—this is necessary to yield a good resolution of v_z. An ultrafast ion image detector consists of two microchannel plates, fast phosphor screen and a gateable intensified charge-coupled-device (ICCD) camera. The time resolution of this type of detector is about 5 ns. Conventional ion velocity mapping method uses high extraction field that compresses the t_r spread to a few nanoseconds. We use instead a weak extraction field to expand t_r to a few hundred nanoseconds in order to achieve a good v_z resolution. One problem arising from the weak extraction field is that the image easily becomes too big—bigger than the detector dimensions. To overcome this problem, an extended ion optics is then adapted for post acceleration after the focus-lens region. The computer simulation of our ion optics (by the SIMION program)[19] is depicted at Fig. 3. By using a soft focusing design (the curvature of the electric potential contour is small), a large ion cloud can be focused. Hence larger signals can be obtained by collecting ions from a bigger volume. Moreover, the focusing condition becomes less sensitive to the ion initial positions, resulting in a more stable operation.

3.3　Experimental data analysis

After a raw image was acquired, the velocity calibration was performed according to the pixel numbers and the ion time of flight. Since the image is taken with time-slicing through the center of the Newton sphere, the ion events of $v_z=0$ are selected. The velocity calibration corresponds to transforming the (x, y) spatial pixel to (v_x, v_y) in the velocity space.

In a crossed molecular beam experiment, two molecular beams cross each other over the time scale of ten microseconds. Within this crossing period, fast recoil products may fly away from the laser detection zone while the slow products stay. Therefore, the overall detection efficiency depends heavily on the product laboratory velocities. A computer program is written to simulate the detection efficiency, in which the spatial and temporal distributions of the molecular beams and the laser beam are explicitly taken into account. The detection sensitivity of products of a given laboratory velocity is calculated. The sensitivity map is then obtained by interpolation of few hundred grid points in

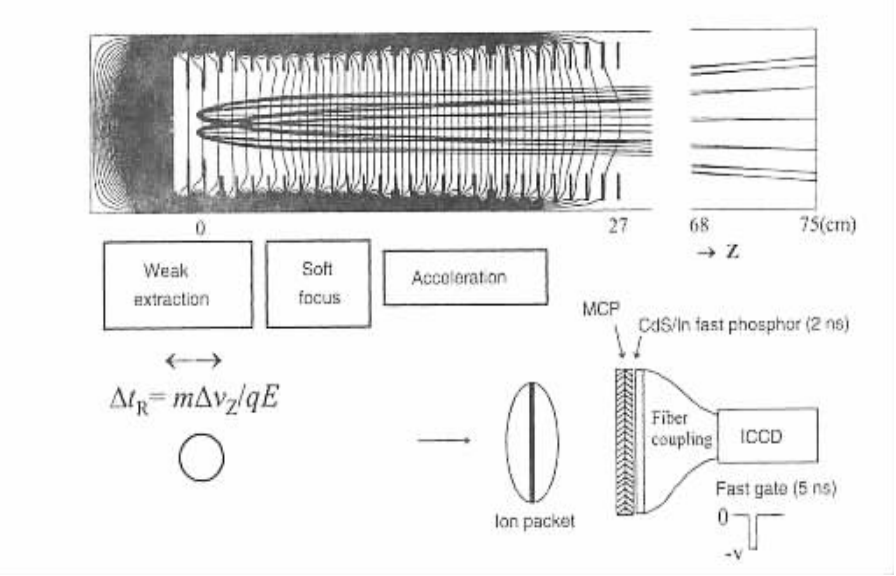

Fig. 3 The computer simulation (using the SIMION program) of the ion optics setup
The two exemplified ion point-sources are separated by 10 mm. The velocity mapping condition brings the trajectories from the two ion sources to the same point on the detector plane if they have the same transverse velocity component. Different positions on the detector plane are from ions with different initial transverse velocities, regardless of their initial positions. The schematics of the image detector with an ultrafast shutter is also shown.

the velocity space (v_x, v_y) [19]. After the sensitivity correction, the product velocity image reveals the distribution in the velocity space that should be symmetric with respect to the relative velocity of the reactants. Different seeding gases will give different F-atom beam speeds, but the same collisional energy can be maintained by adjusting the intersection angles between the molecular beams. Also the angle between the laser beam and the molecular beams can be varied. If the sensitivity correction is done correctly, the results should be invariant to the experimental geometries. We have tested the program and found that it meets this criterion successfully. In the field of reaction dynamics, this sensitivity correction is usually called density-to-flux transformation, which emphasizes the fact that the laser spectroscopic probe measures the density (or concentration) of the molecules, whereas the desired quantity is the flux of the products. The time-sliced velocity imaging approach simplifies considerably the treatment of this transformation.

The ideal time-sliced ion velocity image represents the distribution of ions in the velocity space $(v_x, v_y, v_z = 0)$. Practically, a small time-gate is used to select ions with $-\triangle v/2 < v_z < \triangle v/2$, where $\triangle v$ is the velocity width corresponding to the time-gate. For small enough $\triangle v$, the signal is linearly proportional to $\triangle v$. Therefore, a raw image corresponds to the quantity of

$$\int_{-\triangle v/2}^{\triangle v/2} \mathrm{d}v_z \left(\mathrm{d}\sigma/\mathrm{d}v_x\mathrm{d}v_y\mathrm{d}v_z\right) \cong \left(\mathrm{d}\sigma/\mathrm{d}v_x\mathrm{d}v_y\mathrm{d}v_z\right)\triangle v \quad (13)$$

If a constant time-gate is used to keep $\triangle v$ the same, the latter becomes irrelevant. Since $\mathrm{d}\sigma/\mathrm{d}v_x\mathrm{d}v_y\mathrm{d}v_z$ is the population density in the velocity space, it should be independent of the coordinate systems. We can then transform the data into a polar coordinate (v, θ, ϕ) through

$$\mathrm{d}\sigma/\mathrm{d}v_x\mathrm{d}v_y\mathrm{d}v_z = \mathrm{d}\sigma/v^2\mathrm{d}v\sin\theta\mathrm{d}\theta\mathrm{d}\phi \quad (14)$$

Hence, a simple multiplication of the corrected images by v^2 in the center-of-mass frame suffices to obtain the conventional velocity flux map that shows the quantity of $\mathrm{d}\sigma/\mathrm{d}v\sin\theta\mathrm{d}\theta\mathrm{d}\phi$, i. e.,

$$\mathrm{d}\sigma\mathrm{d}v\sin\theta\mathrm{d}\theta\mathrm{d}\phi = v^2\left(\mathrm{d}\sigma/\mathrm{d}v_x\mathrm{d}v_y\mathrm{d}v_z\right) \quad (15)$$

Here it should be noted that the symmetry axis of the polar coordinate is not necessary to be the z axis of the Cartesian coordinate. Instead, it is usually chosen to

be the relative velocity direction of the reactants so that the azimuthal symmetry over ϕ is retained.

4 Results and discussions

4.1 Product pair correlation

Taking the $F + CD_4 \rightarrow DF + CD_3$ reaction as a prototype, we have explored several facets of product pair correlation. Examples include the quantum number correlation between two product vibrators at a fixed collisional energy[24], the collisional energy dependences of the correlated DF attributes for a given CD_3 vibrational state[25], the pair-correlated excitation function of $F + CH_4 \rightarrow HF(\nu') + CH_3(\nu = 0)$ reaction[26], and more recently, the CD_3 rotational state-selected pair correlation for the $F + CD_4$ reaction[27].

When the laser wavelength is parked at the peak of the Q branch of the two-photon 0_0^0 vibronic transition ($3p_z \leftarrow\leftarrow X$) of CD_3 (the third photon brings it to $CD_3^+ + e^-$), the low rotational states of the CD_3 ground vibrational state are probed. Fig. 4a shows an exemplified CD_3 product velocity image of $F + CD_4 \rightarrow DF(\nu') + CD_3(0000)$ at 22.6 kJ/mol of collisional energy[24]. Since the internal energy of the CD_3 product has been selected by the probe laser, by energy conservation (see equation (4)) the velocity distribution (also the translational energy distribution) mirrors the internal energy distributions of the DF co-products.

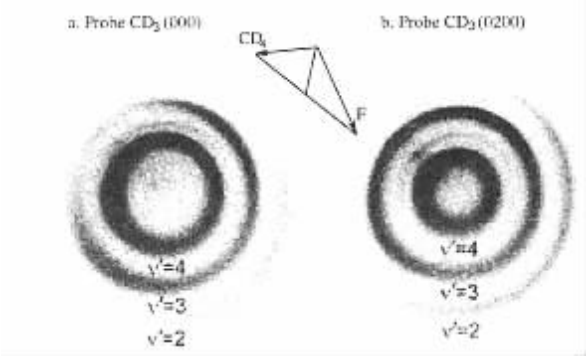

Fig. 4　Examples of raw ion images of the CD_3 products from $F + CD_4$ at 22.6 kJ/mol of collisional energy

a. Probing $CD_3(0000)$ vibrational state, and b. Probing $CD_3(0200)$ vibrational state. The molecular beam velocity diagram (Newton Diagram) and DF product vibrational quantum numbers are indicated.

The ring-like features shown in Fig. 4a can be readily assigned to the DF product vibrational states, $\nu' = 4$, 3, and 2 for the smallest ring and successively larger rings, respectively. The clear separation between the DF vibrational rings indicates low rotational excitation of the DF products.

When the laser wavelength is shifted to the 2_2^0 vibronic transition, the excited $CD_3(0200)$ state with 11.3 kJ/mol of vibrational energy is probed. The product velocity image is shown in Fig. 4b at the same collisional energy as in Fig. 4a. The effect of energy conservation (equation (4)) can be clearly seen when comparing Fig. 4a and Fig. 4b, —the latter displays smaller velocity rings for the same DF vibrational states. More significant is the dependency of the vibrational distributions of the DF co-products on the "tagged" CD_3 vibrational states (the product pair correlation), indicating the correlation between quantum numbers of ν' and ν_2 for the $DF(\nu') + CD_3(0\nu_2 00)$ product pairs. In terms of product state-resolved populations, the pair correlation means the joint probability matrix, $P(\nu', \nu_2)$, which is mxn in dimension for m numbers of vibrational states of DF products and n vibrational states of CD_3 products. The conventional or uncorrelated state distribution corresponds to the averaged form of $P(\nu', \nu_2)$, i.e. $P(\nu) = \Sigma_{\nu 2} P(\nu', \nu_2)$ or $P(\nu_2) = \Sigma_{\nu'} P(\nu', \nu_2)$, which can only have maximal $m + n$ quantities even if both product state distributions are measured. Obviously, it is not feasible to reconstruct the full $P(\nu', \nu_2)$ matrix from the information of $P(\nu')$ and $P(\nu_2)$ alone. Only under limiting cases can the product distributions display no correlation between two molecular products. One example is the spectator case in which a group of atoms plays little role in a reaction and becomes one of the products. Another example is the statistical case, for which the product pair correlation may not convey much additional information about dynamics, as it can be largely predicted by statistical models based on energy and angular momentum constraints.

It is interesting to compare the conventional HF state distribution[28] with our correlated HF state distribution of $CH_3(\nu = 0) + HF(\nu')$[26]. The former is

peaked at $\nu' = 2$ and the latter is peaked at $\nu' = 3$ at collisional energies near 7.5 kJ/mol. Analog to the F + CD_4 case for which higher CD_3 ν_2-excitation is preferentially correlated to lower DF ν'-excitation[24], the uncorrelated HF (summed over all CH_3 states) should have lower vibrational excitation than the HF distribution that is correlated with $CH_3(\nu = 0)$.

The product angular distributions or differential cross sections are clearly revealed even just from the casual inspection of the raw images. There are some common features for Fig. 4a and Fig. 4b. For example, both DF($\nu' = 4$) + CD_3(0000) and DF($\nu' = 4$) + CD_3(0200) product pairs show a very sharp forward peak. The DF($\nu' = 2$) + CD_3($0\nu_2 00$) pairs are backward scattered. Here, we define the 0° angle (or the forward direction when probing CD_3) as the direction of the relative velocity vector, $\mathbf{g} = \mathbf{v}_{CD4} - \mathbf{v}_F$ in the center-of-mass frame. There are also significant differences between Fig. 4a and Fig. 4b. Obviously, the angular distribution of DF($\nu' = 3$) + CD_3(0000) is mostly in the backward and sideways directions, but that of DF($\nu' = 3$) + CD_3(0200) is shifted to forward-sideways and has a sharp forward peak. It is quite remarkable to see that the product angular distributions vary so dramatically with their vibrational quantum number pairs — from a sharp forward peak for DF($\nu' = 4$) + CD_3(ν_2) to backward scattering for DF($\nu' = 2$) + CD_3(ν_2). Besides a strong dependency on the DF vibrational quantum numbers, the product angular distributions depends also significantly on the CD_3 vibrational quantum numbers, for which the energy separation per quantum is 5.9 kJ/mol, relatively small with respect to the 33.4 kJ/mol spacing of the DF vibrational levels.

The transition state of the F + CD_4 reaction is of an early barrier with an elongated D-F bond in a nearly linear F-D-C geometry[29]. The observation of a strong vibrational population inversion of the DF products and a weak excitation of the umbrella mode of CD_3 products is therefore not too surprising[30]. In addition to the product state distributions, we have observed an anticorrelation between the quantum numbers of the two product vibrators. This anticorrelation indicates that the motion at and after the transition state is more subtle than just the above considerations of the energetics and structure of the transition state. It is believed that the outcome of a reaction will be mostly governed by the concerted motion of atoms across the transition state. The correlation between the two product vibrators undoubtedly reveals more dynamical features of the reaction, especially when the concerted motion of atoms is of concern. In that sense, the product pair-correlation may provide the most lucid picture of the transition-state dynamics of a polyatomic reaction. Considering the microscopic reversibility of a reaction, the pair-correlation is intimately related to the concept of mode-specific reactivity. Hence, it will certainly provide a much more rigorous test for the quantum dynamical calculations.

A polyatomic reaction offers an opportunity to address the dynamical questions other than those have been encountered in three-atom reactions. The multiple mode nature of a polyatomic molecule is one of the issues. In the F + CHD_3 → DF + CHD_2 reaction, a Fermi resonance between 4_2 and 3_1 vibrational states of CHD_2 has been discovered[31]. It is interesting to note that this discovery is made from the conclusion of the dynamical observables (the state distributions, angular distributions, collisional energy dependences, etc) rather than from the more conventional spectroscopic analysis.

4.2 Reactive resonance

Reactive resonance is one of the most fascinating phenomena in reaction dynamics. The term resonance refers to a transiently formed metastable that is produced while the reaction is taking place. If we view the occurrence of a chemical transformation as the motion of atoms on a Born-Oppenheimer potential energy surface (PES), the existence of reactive resonance can be traced back to dynamical trapping in wells on the vibrationally adiabatic PES, even when there is no well on the Born-Oppenheimer PES. It is a quantum mechanical phenomenon and is dynamical in origin.

After 20-year debates, the mystery of reactive resonance has recently been unlocked in F + HD → HF + D reaction[7-9,13]. The vibrational quantum numbers of the resonance state of the transient FHD complex have

been assigned as (003), three vibrational quanta in the antisymmetric H – F stretching mode and zero quanta in other modes[13]. The adiabatic separation of the high frequency H – F stretching mode plays an important role in this reactive resonance. For a polyatomic reaction, the reactive resonance is a hitherto unexplored frontier both theoretically and experimentally. Due to high density of states, intramolecular vibrational redistribution (IVR) processes are quite common in polyatomic systems. If there is a reactive resonance in a polyatomic reaction, one might anticipate that the IVR process could have significant effects, for example, in shortening the lifetime of the resonance state and possibly washing out the possible resonance signatures.

By examining several dynamical attributes of F + CH_4 reaction at collisional energies close to the reaction threshold, we have recently presented the first experimental evidence for reactive resonance in this polyatomic reaction[32]. The reactivity near the reaction threshold is significantly enhanced by the resonant tunneling through the reaction barrier of about 2.1 kJ/mol. However, the signature of resonance in this polyatomic reaction turns out to be most clearly revealed in the decay of the resonance state, which is in a highly mode-/state-specific manner. Most notably, the high-frequency symmetric stretching mode ($\nu_1 = 1$) excitation of CH_3 product is observed only at low collisional energies. To put in a simple physical terms, not only is the HF($\nu' = 2$, high j') + CH_3($\nu = 0$) product pair formed (analogous to the HF($\nu' = 2$, high j') + D from the F + HD reaction, but also the HF($\nu' = 2$) + CH_3($\nu_1 = 1$) product pair is produced through a suggested IVR process. Nonetheless, the crust of the resonance formation mechanism appears quite similar for the F + CH_4 and the previously reported F + HD reactions.

5 Conclusions

From the product pair-correlation to the reactive resonance, we have demonstrated that rich information of the polyatomic reaction can be obtained by using the crossed molecular beam method combined with a high resolution ion velocity imaging method. The dual rotating sources, crossed molecular beam apparatus offers a convenient way to study the collisional energy dependence. The combination of REMPI detection and ion velocity imaging is ideal to resolve the product state and angular distributions, and at the same time to obtain the pair-correlated information. At higher collisional energies, more methyl vibrational excitation and less HF/DF vibrational excitation have been observed. The vibrational distributions of HF/DF products show strong anticorrelation to both vibrational and rotational excitation of the methyl co-products. The product angular distributions are very sensitive to the pair-correlation of the product states. Isotope effects have been investigated. The first evidence of reactive resonance in a polyatomic reaction has been uncovered.

Multiple vibrational modes are the characteristics of a polyatomic system. The interaction between the vibrational modes is undoubtedly an important issue. The product vibrational mode correlation indicates which types of motion are active or frozen while the reaction is taking place. The quantum number correlation offers a more quantitative aspect. The correlation information holds great promise to unravel the "extra-atom" complexity of a polyatomic reaction. Theoretical work on these important issues will definitely help our understanding to the polyatomic reactions. We have started to extend this type of study to Cl + CH_4 reaction and OH + CH_4 reaction. It will be highly rewarding to compare this series of abstraction reactions of various barrier heights, exothermicity, transition state locations, etc.

Acknowledgements The authors acknowledge the supports from National Science Council of Taiwan (NSC 92-2113-M-001-044 (JJL) and NSC 92-2113-M-001-040 (KL)) and from Academia Sinica, Taipei, Taiwan.

References

[1] Liu K. *Annu. Rev. Phys. Chem.*, 2001, **52**: 139

[2] Levine R D, Bernstein R B. Molecular Reaction Dynamics and Chemical Reactivity, Oxford Univ. Press, Oxford, 1987.

[3] Fernandez-Alonso F, Zare R N. *Annu. Rev. Phys. Chem.*, 2002, **53**: 67
[4] Schnieder L, Seekamp-Rahn K, Wrede E, Welge K H. *J. Chem. Phys.*, 1997, **107**: 6175
[5] Althorpe S C, Fernandez-Alonso F, Beam B D, Ayers J D, Pomerantz A E, Zare R N, Wrede E. *Nature*, 2002, **416**: 67
[6] Harich S A, Dai D, Wang C C, Yang X, Chao S D, Skodje R T. *Nature*, 2002, **419**: 218
[7] Skodje R T, Skouteris D, Manolopoulos D E, Lee S H, Dong F, Liu K. *Phys. Rev. Lett.*, 2000, **85**: 1206
[8] Liu K, Skodje R T, Manolopoulos D E. *Phys. Chem. Comm.*, 2002, **5**: 27
[9] Lee S H, Dong F, Liu K. *J. Chem. Phys.*, 2002, **116**: 7839
[10] Liu X, Lin J J, Harich S, Schatz G C, Yang X. *Science*, 2000, **289**: 1536
[11] Strazisar B R, Lin C, Davis H F. *Science*, 2000, **290**: 958
[12] Crim F F. *Acc. Chem. Res.*, 1999, **32**: 877
[13] Skodje R T, Skouteris D, Manolopoulos D E, Lee S H, Dong F, Liu K. *J. Chem. Phys.*, 2000, **112**: 4536
[14] Liu K. *Int. Rev. Phys. Chem.*, 2001, **20**: 189
[15] Hudgens J W, DiGiuseppe T J, Lin M C. *J. Chem. Phys.*, 1983, **79**: 571
[16] Child M S. Molecular Collision Theory, Academic Press, New York, 1974.
[17] Scoles G. Atomic and Molecular Beam Methods, Oxford Univ. Press, 1988.
[18] Dong F, Lee S H, Liu K. *J. Chem. Phys.*, 2000, **113**: 3633
[19] Lin J J, Zhou J, Shiu W, Liu K. *Rev. Sci. Instrum.*, 2003, **74**: 2495
[20] Chandler D W, Houston P L. *J. Chem. Phys.*, 1987, **87**: 1445
[21] Heck A J R, Chandler D W. *Annu. Rev. Phys. Chem.*, 1995, **46**: 335
[22] Parker D H, Eppink A T J B. *Rev. Sci. Instrum.*, 1997, **68**: 3477
[23] Wiley W C, McLaren I H. *Rev. Sci. Instrum.*, 1995, **26**: 1150
[24] Lin J J, Zhou J, Shiu W, Liu K. *Science*, 2003, **300**: 966
[25] Zhou J, Lin J J, Shiu W, Liu K. *J. Chem. Phys.*, 2003, **119**: 4997
[26] Shiu W, Lin J J, Liu K, Wu M, Parker D H. *J. Chem. Phys.*, 2004, **120**: 117
[27] Zhou J, Lin J J, Liu K. *J. Chem. Phys.*, 2004, **120**: 5863
[28] Harper W W, Nizkorodov S A, Nesbitt D J. *J. Chem. Phys.*, 2000, **113**: 3670
[29] Corchado J C, Espinosa-Garcia J. *J. Chem. Phys.*, 1996, **105**: 3152
[30] Kornweitz H, Persky A, Levine R D. *Chem. Phys. Lett.*, 1998, **289**: 125
[31] Zhou J, Lin J J, Liu K. *J. Chem. Phys.*, 2003, **119**: 8289
[32] Shiu W, Lin J J, Liu K. *Phys. Rev. Lett.*, 2004, **92**: 103201